

Spatially Isolated Noble-Metal-Free Redox Cocatalysts on CdS Nanorods for Increased Photocatalytic Hydrogen Generation

Xiaomeng Zhang¹⁺, Gege Zhao¹⁺, Zhongfei Li¹, Liang Zhu¹, Yingpeng Cheng¹, Haiwei Du¹, Chuhong Zhu¹, Ya Dang³, Daochuan Jiang^{1,3*} and Yupeng Yuan^{1,2*}

¹School of Materials Science and Engineering, Anhui University, Hefei 230601, China

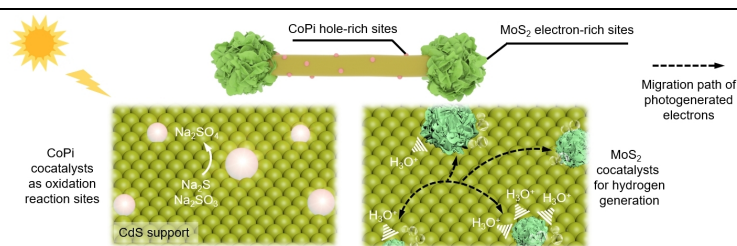
²Key Laboratory of Structure and Functional Regulation of Hybrid Materials (Anhui University), Ministry of Education, and Energy Materials and Devices Key Lab of Anhui Province for Photoelectric conversion, Anhui University, Hefei 230601, China

³Anhui Chinaherb Flavors & Fragrances Co., Ltd., Bengbu 233400, China

ABSTRACT Spatially isolated oxidation and reduction cocatalysts on a semiconductor can realize efficient charge separation and thereby lead to increased photocatalytic hydrogen generation. However, the effective preparation of such photocatalysts has proven challenging. Herein, we report the facile synthesis of a novel noble-metal-free CdS/MoS₂/CoPi ternary photocatalyst via a visible light-induced synthesis route, in which MoS₂ re-

duction cocatalysts were precisely grown on the two terminals of CdS nanorods, while CoPi oxidation cocatalysts were preferentially anchored onto the sidewalls of CdS nanorods. Such spatially isolated MoS₂ and CoPi redox cocatalysts endow CdS nanorods with a rapid charge separation, which enhances their hydrogen generation activity. The CdS/MoS₂/CoPi photocatalyst with optimized CoPi amount achieves the highest H₂ generation rate of 206 $\mu\text{mol/h}$, which is 21 and 2 times higher than that achieved by using CdS alone (9.7 $\mu\text{mol/h}$) and CdS/MoS₂ (105 $\mu\text{mol/h}$), respectively. The present work highlights the effectiveness of the spatial isolation of reduction and oxidation sites for efficient charge separation and thereby provides a promising strategy for the preparation of highly active photocatalysts.

Keywords: spatially isolated cocatalyst, light-induced synthesis, cadmium sulfide, photocatalytic H₂ generation



INTRODUCTION

Photocatalytic hydrogen (H₂) generation from water splitting has been widely recognized as a sustainable and promising reaction toward the efficient conversion of solar energy into chemical fuels.^[1–4] Among various photocatalysts for photocatalytic H₂ generation, CdS has received intensive studies mainly owing to its narrow bandgap, suitable energy position, low cost, and easy preparation.^[5–10] Nevertheless, the photocatalytic performance of pristine CdS is quite poor, which is predominantly due to severe charge recombination. On the other hand, the lack of active sites also confers CdS a low efficiency for redox reaction.^[11] To this end, anchoring suitable redox centers, particularly dual cocatalysts, on the surface of CdS can simultaneously provide active sites for proton reduction and accelerate charge separation.^[12,13] To date, various dual cocatalysts, such as Pt-PdS,^[14] PdS-NiS, MoS₂-NiS,^[15] Ag₂S-NiS,^[16] CoO_x-MoS₂,^[17] and MoS_x-Co₃O₄,^[18] have been extensively examined on CdS semiconductors for increased photocatalytic performance. It is worth noting that one-dimensional (1D) CdS nanorods can vectorially transfer electrons along the length direction and thus have been generally used as substrates to anchor various cocatalysts. Despite the great progress of dual cocatalysts, the following two issues still exist in the reported literature. First, the reduction cocatalysts reported mainly rely on noble metals, which are relatively scarce in nature and high-cost for large-scale applications.^[19,20] Second, most of the dual cocatalysts reported were randomly distributed on the sur-

face of CdS owing to their anchoring route (e.g., chemical precipitation or absorption), which resulted in a less increased separation of photogenerated electrons and holes.^[17,21] Clearly, it is highly desirable to anchor spatially isolated noble-metal-free redox dual cocatalysts on CdS nanorods, which has not yet been largely investigated.

Herein, we report the facile preparation of a noble-metal-free CdS/MoS₂/CoPi nanorod ternary photocatalyst with a spatially isolated MoS₂ reduction cocatalyst and CoPi oxidation cocatalyst via a viable light-induced synthesis route. Specifically, MoS₂ nanosheets were first selectively grown on the two terminals of CdS nanorods by a simple solvothermal method. Afterwards, the MoS₂-decorated CdS nanorods were further anchored with CoPi nanoparticles on the sidewalls via a facile photooxidation deposition method. CoPi was preferentially deposited on the sidewalls of CdS nanorods from the oxidation of Co²⁺ ions by photogenerated holes, which is primarily transferred along the direction perpendicular to 1D CdS nanorods. Such spatially isolated MoS₂ reduction cocatalyst and CoPi oxidation cocatalyst render CdS nanorods with a significantly increased charge separation, thereby leading to a dramatically improved photocatalytic H₂ generation rate of 206 $\mu\text{mol/h}$, which is more than 21 times higher than that obtained by using pristine CdS nanorods.

RESULTS AND DISCUSSION

The preparation of noble-metal-free CdS/MoS₂/CoPi nanorods is schematically illustrated in Figure 1a. CdS nanorods were first sol-

thermally synthesized in the presence of ethylenediamine (EDA), which served as the surface ligands to cover the surface of the CdS nanorods, as revealed by the FT-IR spectrum (Figure S1).^[22] The CdS thus obtained has a rod-shaped morphology with length of $\sim 1\ \mu\text{m}$ and diameter of $\sim 50\ \text{nm}$, as shown in Figure 1b and Figure S2. Afterwards, the MoS₂ reduction cocatalyst was grown on the unpurified CdS nanorods via a facile solvothermal route in a diethylenetriamine (DETA) aqueous solution. Owing to the strong repulsion between the amine groups on the surface of unpurified CdS nanorods and the Mo precursor coordinated with DETA, the growth of MoS₂ at the lateral surface of CdS nanorods was hindered. However, the growth of MoS₂ can occur at the two terminals of the nanorod due to the fact that both anionic sulfur donors and cationic Mo donors can be captured by the chemical interaction with the Cd-terminated facet and S-terminated facet on (001)-oriented CdS nanorods.^[23] In this way, the location of MoS₂ can be regulated. The selective growth of MoS₂ on the two terminals of CdS nanorods is first visualized by TEM and SEM images, as shown in Figure 1c and Figure S2. Very impressively, the CdS/MoS₂ composites have a dumbbell-shaped morphology, in which the flower-like MoS₂ flakes were selectively capped on

the two terminals of CdS nanorods. Subsequently, CoPi oxidation cocatalysts were anchored on CdS/MoS₂ nanorods via a photooxidation deposition route under an inert Ar atmosphere for 3 hours. Given the fact that the photogenerated holes are primarily transferred along the direction perpendicular to 1D structure,^[24] the holes will migrate to the lateral surface of CdS/MoS₂ nanorods and be consumed by the Co²⁺ in the KPi solution, leading to the preferential deposition of CoPi oxidation cocatalyst. Despite the almost identical morphology with CdS/MoS₂ (Figure 1d), the deposition of CoPi can still be confirmed by EDS analysis (Figure 1e), which illustrates the signals of Cd, S, Mo, Co, and P elements. To further verify the deposition of MoS₂ and CoPi on CdS nanorods, high-resolution transmission electron microscopy (HRTEM) of CdS/MoS₂/CoPi-5 was recorded. In the terminal surface of the nanorod (Figure 1f), the HRTEM images illustrate interplanar spacing of 0.33 and 0.625 nm (Figure 1g-j), which are assigned to the facets of (001) for CdS and (002) for MoS₂, respectively.^[23] For the lateral surface of the nanorod, some tiny particles with a size of $\sim 5\ \text{nm}$ can be clearly observed, which can be attributed to the CoPi cocatalysts (Figure 1k). Notably, CoPi nanoparticles are amorphous, as exemplified by the lack of lattice fringes in

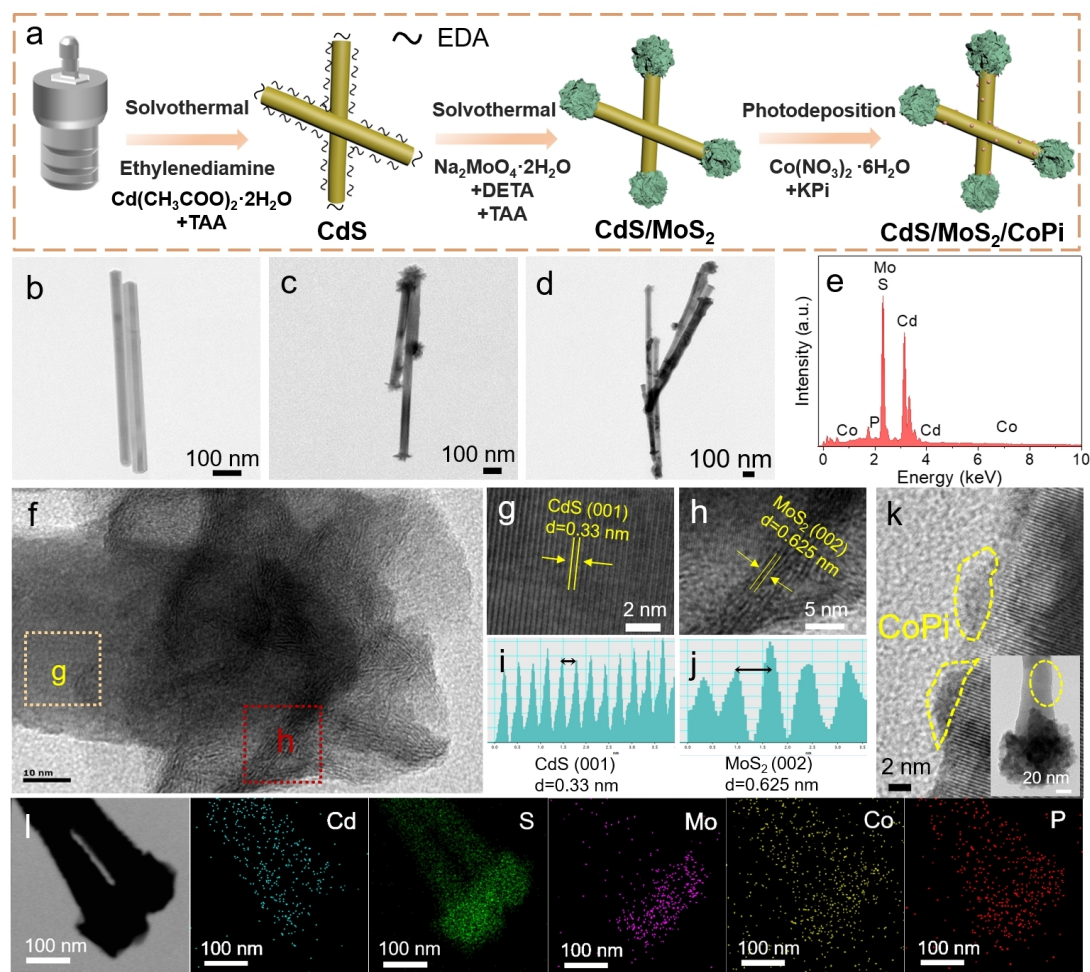


Figure 1. (a) Schematic illustration of the synthesis of the CdS/MoS₂/CoPi ternary photocatalyst; TEM images of CdS (b), CdS/MoS₂ (c), and CdS/MoS₂/CoPi-5 (d); (e) EDX spectrum of the CdS/MoS₂/CoPi-5 sample. HRTEM images of the terminal surface (f-j) and lateral surface (k) of the CdS/MoS₂/CoPi-5 sample. (l) Elemental mapping of the CdS/MoS₂/CoPi-5 sample.

HRTEM.^[25] The distribution of the elements in CdS/MoS₂/CoPi-5 was studied by element mapping (Figure 1l). As expected, Mo was selectively located at the terminals of the nanorod. Interestingly, the signals of Co and P can be observed at both the lateral and terminal surfaces of the nanorod, suggesting some CoPi nanoparticles were also deposited on MoS₂. The selected area EDX spectra on one representative CdS/MoS₂/CoPi-5 nanorod show that the content of Co species in the lateral surface of the rod is 2 times higher than that in the terminal surface (Figure S3), suggesting that Co species were mainly deposited on the sidewalls of the nanorod. Accordingly, it is reasonable to conclude that the preferential deposition of CoPi at the lateral surface of CdS nanorods owing to the photogenerated holes tends to separate perpendicularly to the rod.

X-ray diffraction (XRD) analysis was used to reveal crystal structures of the as-prepared samples. As shown in Figure 2a, pristine CdS shows a hexagonal phase structure (PDF#77-2306).^[26] No alterations occur in the XRD peak intensity and location after loading MoS₂ and CoPi (Figure 2a and Figure S4). The missing peaks of MoS₂ and CoPi in the XRD patterns are probably due to the weak crystallinity and relatively low amounts. The introduction of MoS₂ and CoPi imparts CdS with increased light harvesting, as shown by UV-vis diffuse reflectance spectra (Figure 2b). All samples display almost the same light absorption edge of ~520 nm, corresponding to a band-gap energy of 2.4 eV for CdS.^[27] Notably, the CdS/MoS₂ and CdS/MoS₂/CoPi samples exhibit elevated light absorption intensities in the range of 520–700 nm, further supporting the introduction of MoS₂ and CoPi onto CdS na-

norods. The light absorption spectra are in line with the color change from yellow for CdS to dark green for CdS/MoS₂/CoPi (inset in Figure 2b).

X-ray photoelectron spectroscopy (XPS) was further carried out to analyze the surface chemical composition and electronic states of the as-prepared samples. The signals of Cd, S, Mo, Co, P, and O in the XPS survey spectrum of CdS/MoS₂/CoPi-5 confirm the introduction of MoS₂ and CoPi onto CdS (Figure S5), in good agreement with EDS analysis (Figure 1e). In the high-resolution Cd 3d XPS spectra (Figure 2c), pristine CdS shows two peaks at binding energies of 404.97 and 411.65 eV, which can be ascribed to Cd 3d_{5/2} and Cd 3d_{3/2}, respectively. Noticeably, the deposition of MoS₂ positively shifts the XPS peak of Cd 3d to a high binding energy of 0.35 eV, suggesting a low electronic density around Cd sites in the CdS/MoS₂ sample. In addition, anchoring CoPi positively shifts the Cd 3d_{3/2} peak to a high binding energy by 0.1 eV compared to that of CdS/MoS₂. The peaks of Mo 3d_{5/2} and Mo 3d_{3/2} for the CdS/MoS₂/CoPi sample are approximately 228.5 and 232.2 eV, respectively, which shift to a low binding energy of 0.1 eV (Figure 2d). The shifts of the binding energy for Cd 3d and Mo 3d confirm the strong electronic interaction owing to the intimate interaction among CdS, MoS₂, and CoPi at their interfaces, which is favorable for charge transfer across the interfaces in the CdS/MoS₂/CoPi sample. For the Co 2p spectrum (Figure 2e), two peaks at binding energies of 781.6 and 797.4 eV are assigned to Co 2p_{3/2} and 2p_{1/2}, respectively. This result is consistent with the CoPi species reported in the literature.^[17] The P 2p signal was fitted into one peak with a binding energy of 133.45 eV, as shown in Figure 2f, which is the characteristic binding energy of P in the phosphate group.^[21] The high-resolution XPS spectrum of S exhibits two typical peaks at 161.6 and 162.8 eV (Figure S6), suggesting the existence of S²⁻ ions in all samples.

To reveal the effect of spatially separated reduction and oxidation cocatalysts on charge separation, photocatalytic H₂ generation experiments were performed in a mixed solution of 0.25 M Na₂S and 0.35 M Na₂SO₃ under irradiation with a 300 W Xenon lamp equipped with a cutoff filter ($\lambda > 420$ nm) to provide visible light. Pristine CdS exhibits a low photocatalytic H₂ generation rate of 9.7 $\mu\text{mol/h}$ owing to the lack of cocatalysts (Figure 3a), which would result in rapid charge recombination. The deposition of MoS₂ reduction cocatalyst significantly improves the H₂ generation up to 105 $\mu\text{mol/h}$, which is ca. 3.1 times higher than that of Pt/CdS, suggesting a dramatically increased separation of electron-hole pairs in the presence of MoS₂ as reduction cocatalyst. Very impressively, codeposition of spatially isolated MoS₂ reduction cocatalysts and CoPi oxidation cocatalysts could further enhance the photocatalytic H₂ generation rate (Figure S7), supporting that such spatial separation of reduction and oxidation cocatalysts can effectively increase charge separation. The CdS/MoS₂/CoPi-5 sample with the optimized CoPi amount offers the highest H₂ generation rate of 206 $\mu\text{mol/h}$ (Figure 3a), which is approximately 21 times higher than that obtained by using pristine CdS. In stark contrast to spatially isolated MoS₂ and CoPi, the CdS/MoS₂/CoPi ternary photocatalyst with randomly deposited MoS₂ and CoPi cocatalysts (labeled as R-CdS/MoS₂/CoPi-5, Figure S8) shows a H₂ generation rate of only 113 $\mu\text{mol/h}$ (Figure 3a),

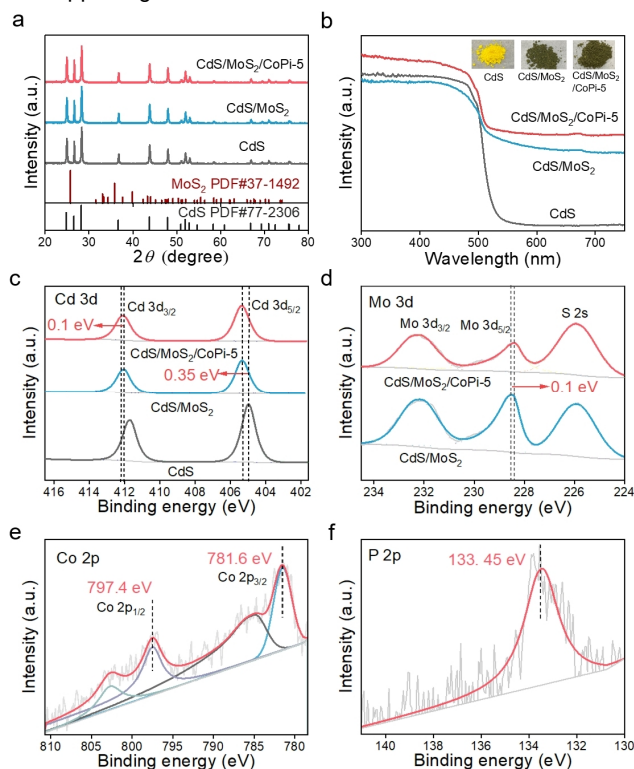


Figure 2. XRD patterns (a) and UV-visible absorption spectra (b) of CdS, CdS/MoS₂, and CdS/MoS₂/CoPi. High-resolution XPS spectra of Cd 3d (c), Mo 3d (d), Co 2p (e), and P 2p (f) of the as-prepared samples.

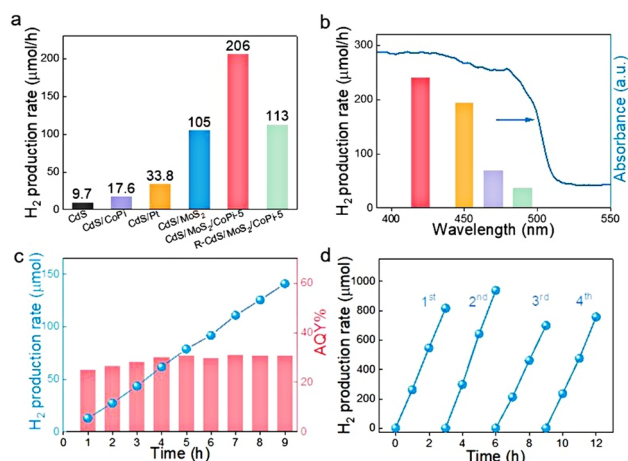


Figure 3. (a) Photocatalytic H₂ generation rate of various samples. (b) Wavelength-dependent H₂ generation of the CdS/MoS₂/CoPi-5 sample. (c) The H₂ generation profile with prolonged time in hours and corresponding apparent quantum yield (AQY) of the CdS/MoS₂/CoPi-5 sample under irradiation with monochromatic light with a wavelength of 420 nm. (d) Cycling H₂ generation of the CdS/MoS₂/CoPi-5 sample. Reaction conditions: 5 mg of catalyst; (a), (b), and (d) 20 mL of Na₂S (0.25 M) and Na₂SO₃ (0.35 M) in water. (c) 20 mL of Na₂S (0.75 M) and Na₂SO₃ (1.05 M) in water.

which is near half of the H₂ generation rate of the CdS/MoS₂/CoPi-5 sample. This reduced H₂ generation rate highlights the advantages of the spatial separation of reduction and oxidation cocatalysts, which is favorable for efficient charge separation and thus results in an increased photocatalytic H₂ generation rate. Wavelength-dependent H₂ production was also conducted to reveal the contribution of light absorption to photocatalytic performance (Figure 3b). The H₂ production rate progressively decreases with extended light wavelength, and negligible H₂ generation is detected when the wavelength of incident light is above ~520 nm, the absorbance edge of pristine CdS. This result clearly suggests that the light absorption in the range of 520–750 nm that was caused by MoS₂ and CoPi cocatalysts had negligible contributions to H₂ production. In addition, the H₂ production rate is highly sensitive to the concentration of Na₂S and Na₂SO₃ sacrificial reagents (Figure S9). In detail, the H₂ generation rate increases with the concentration of sacrificial reagents and stops increasing at concentrations of Na₂SO₃ and Na₂S above 1.05 and 0.75 M, respectively. The apparent quantum yield (AQY) was evaluated under irradiation with monochromatic light of 420 nm in a 20 mL aqueous solution containing 1.05 M Na₂SO₃ and 0.75 M Na₂S. As shown in Figure 3c, the average AQY was determined to be ~30.9% within 9 hours, which is better than that of many recently reported CdS-based photocatalysts in the literature (Table S1). We further evaluated the long-term H₂ generation by testing the cycling H₂ generation of the CdS/MoS₂/CoPi-5 sample. As shown in Figure 3d, the CdS/MoS₂/CoPi-5 sample exhibits a similar H₂ generation rate in four consecutive cycles, suggesting relatively excellent stability. This durable H₂ generation was further confirmed by a nearly linear increment of H₂ produced within 25 hours (Figure S10). Moreover, XRD analysis and SEM observations display negligible changes after photocatalytic H₂ generation

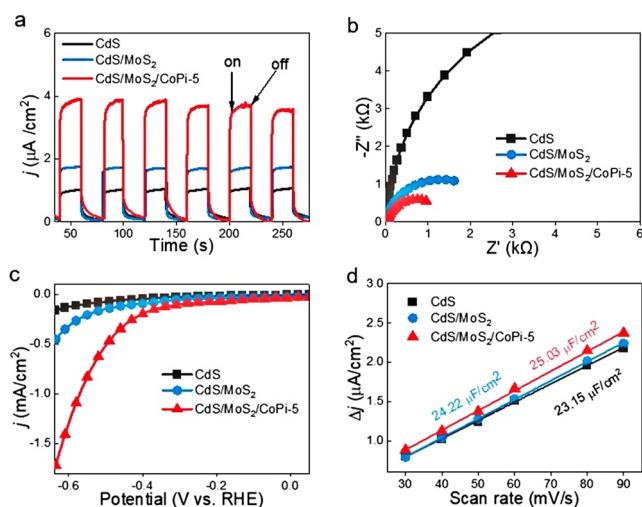


Figure 4. Electrochemical measurements of CdS, CdS/MoS₂, and CdS/MoS₂/CoPi-5 samples. Transient photocurrent response (a). EIS spectra (b). LSV curves (c). C_{dl} measurements (d).

reactions (Figure S11, Figure S12), further verifying the stability of the CdS/MoS₂/CoPi photocatalyst.

We then performed electrochemical measurements of CdS/MoS₂/CoPi samples to uncover the mechanism of increased photocatalytic H₂ generation. The transient photocurrent density of the CdS/MoS₂/CoPi-5 sample was significantly larger than that of CdS/MoS₂ and pristine CdS (Figure 4a), illustrating the effectiveness of the spatial isolation of MoS₂ and CoPi redox cocatalysts on efficient charge separation. This result was further supported by the electrochemical impedance analysis, where the CdS/MoS₂/CoPi-5 sample has a smaller charge transfer resistance (R_{ct}) than CdS and CdS/MoS₂, as exemplified by the smaller arc radius (Figure 4b). The larger photocurrent and smaller photocarrier transfer resistance are favorable for an increased photocatalytic performance, which was further revealed by the LSV measurements. The cathodic current density of the CdS/MoS₂/CoPi-5 sample outperforms those of CdS/MoS₂ and CdS in the entire range of tested potentials (Figure 4c). The double-layer capacitance (C_{dl}) was used to estimate the electrochemically active surface area (ECSA) (Figure S13), and the CdS/MoS₂/CoPi-5 sample possesses a larger C_{dl} of 25.03 μF/cm², indicating more exposed active sites (Figure 4d).^[28]

To directly track the efficient charge separation and transfer behavior owing to the spatially separated MoS₂ and CoPi dual cocatalysts, the as-prepared samples were further investigated by single-particle PL imaging technology. The wavelength of the excitation laser was chosen at 405 nm. Figure 5a–c shows the PL image of pristine CdS, CdS/MoS₂, and CdS/MoS₂/CoPi-5, respectively, and the corresponding PL spectra are shown in Figure 5d. An intensive PL peak centered at ~510 nm was observed for pristine CdS to give its band gap of ~2.43 eV.^[29] After the selective growth of MoS₂ nanosheets as the reduction cocatalyst in the two terminals of CdS nanorods, there is no significant change in the position of the emission peak, while the intensity of individual nanorods was remarkably quenched, revealing the inhibition of re-

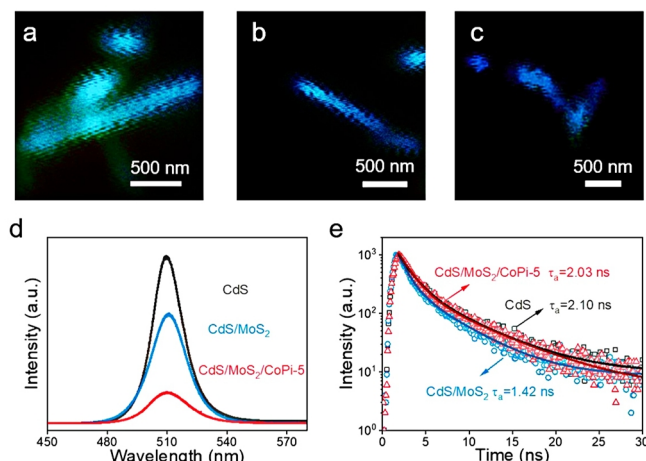


Figure 5. Single-particle PL images of CdS (a), CdS/MoS₂ (b), CdS/MoS₂/CoPi-5 (c). PL spectra (d) and TRPL spectra (e) of the CdS, CdS/MoS₂, and CdS/MoS₂/CoPi-5 samples.

combination of charge carriers due to the efficient charge transfer from CdS to MoS₂. Importantly, when both MoS₂ nanosheets and CoPi nanoparticles were selectively decorated on the different sites of CdS nanorods, the PL intensity of CdS/MoS₂/CoPi-5 sharply decreased, as demonstrated by the much darker PL image of individual nanorods shown in Figure 5c. To further probe the charge transfer dynamics, the charge carrier lifetimes of the pristine CdS, MoS₂/CoPi, and CdS/MoS₂/CoPi-5 samples were measured by time-resolved PL (TRPL) spectroscopy (Figure 5e). Pristine CdS exhibits an average lifetime of 2.1 ns, which is longer than that of CdS/MoS₂ (1.42 ns). This reduced lifetime in CdS/MoS₂ is mainly due to the rapid transfer of photogenerated electrons from CdS to MoS₂. Notably, CoPi decoration prolongs the lifetime to 2.03 ns, which is the result of rapid hole transfer, thereby suppressing the recombination of electrons and holes in the CdS/MoS₂/CoPi-5 sample.^[22]

The conduction band positions were calculated by Tauc plots and valence band spectra (Figure S14). Based on the above-mentioned results, the mechanism for enhanced photocatalytic H₂ generation is proposed in Figure 6. Under visible light irradiation, the electrons are excited from the valence band of CdS nanorod to its conduction band, and then the photogenerated electrons

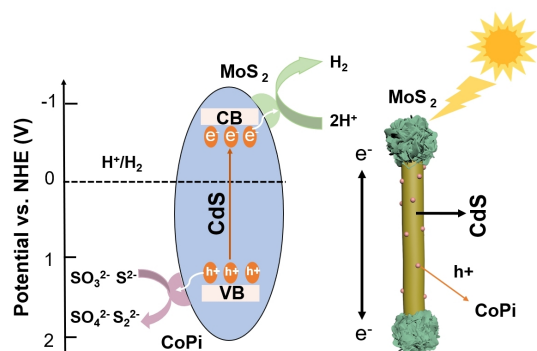


Figure 6. Scheme of the proposed mechanism for photocatalytic hydrogen production on CdS nanorods with spatial separation of dual-cocatalysts.

transfer along the nanorod and are withdrawn by the MoS₂ reduction cocatalyst in the two terminals of the nanorod; while the holes in the valence band transmit to the sidewalls of the nanorod and move to the CoPi oxidation cocatalyst preferentially deposited on the lateral surface of CdS nanorod. In this configuration, the photo-generated electrons and holes are spatially separated at different surface active sites, leading to efficient charge separation, which contributes to the dramatically improved photocatalytic H₂ generation.

CONCLUSION

In summary, a novel CdS/MoS₂/CoPi ternary photocatalyst with intimate interfacial contact was synthesized by selective decoration of MoS₂ as the reduction cocatalyst and CoPi as the oxidation cocatalyst on the two terminals and the lateral surface of CdS nanorods, respectively. The construction of spatially separated MoS₂ and CoPi dual cocatalysts on well-defined CdS nanorods enables the oriental migration and capture of the photogenerated charge carriers of CdS, thereby achieving efficient charge separation and transfer. Owing to the unique architecture and strong synergistic effect between the dual cocatalysts, the optimal CdS/MoS₂/CoPi photocatalyst exhibited a 21-fold enhancement in the H₂ production rate with good stability compared to pristine CdS. The present study provides a promising strategy to design efficient and cost-effective photocatalysts for solar fuel production.

EXPERIMENTAL

Materials. EDA (99%), cadmium diacetate dihydrate (Cd(CH₃COO)₂·2H₂O, 99%), DETA (97%), sodium molybdate dihydrate (Na₂MoO₄·2H₂O, 99%), thioacetamide (TAA, 99%), cobaltous nitrate hexahydrate (Co(NO₃)₂·6H₂O, 99%), sodium dihydrogen phosphate (NaH₂PO₄, 99%), and dibasic sodium phosphate (Na₂HPO₄, 99%) were commercially available and used without further purification.

Synthesis of CdS Nanorods. In a typical procedure, 1.6 g cadmium acetate dihydrate (Cd(CH₃COO)₂·2H₂O) and 1 g TAA (CH₃CSNH₂) were added into a 100 mL Teflon-lined autoclave filled with 60 mL of EDA as the solvent. After stirring for 30 min, the solution was sealed and heated at 180 °C for 16 h and then allowed to cool to room temperature naturally. The obtained amine-functionalized CdS was separated by centrifugation, and the unwashed CdS was dried in an oven at 80 °C.

Synthesis of CdS/MoS₂. A total of 0.6 g CdS nanorods without washing treatment, 1 g TAA and 0.3 g sodium molybdate (Na₂MoO₄·2H₂O) were dispersed in a mixed solvent containing 30 mL DETA. After stirring for 1 h, the homogeneous solution was transferred into a 50 mL Teflon-lined autoclave, which was sealed and maintained at 180 °C for 21 h and then naturally cooled to room temperature. The resulting precipitates were collected by centrifugation and washed with ethanol and DI water three times until the organic molecules were completely removed and then dried under vacuum at 80 °C overnight.

Synthesis of CdS/MoS₂/CoPi. Typically, 50 mg of CM sample was dispersed in a 30 mL aqueous neutral buffer solution containing 0.1 M sodium phosphate and a certain amount of 0.02 M co-

balt nitrate hexahydrate ($\text{Co}(\text{NO}_3)_2 \cdot 6\text{H}_2\text{O}$). After nitrogen degassing for 30 min, the suspension was illuminated with visible light for 3 h in a nitrogen atmosphere. After that, the sample was collected by centrifugation, washed with water and ethanol three times, and dried at 80 °C in air. The nominal atomic ratios of Co to Cd (designated R) were 1, 3, 5, and 9, and the obtained samples were labeled as CoPi/MoS₂/CdS-1, CoPi/MoS₂/CdS-3, CoPi/MoS₂/CdS-5 and CoPi/MoS₂/CdS-9.

Synthesis of R-CdS/MoS₂/CoPi. The synthesis procedure of the CdS/MoS₂/CoPi ternary photocatalyst with randomly deposited MoS₂ and CoPi cocatalysts (R-CdS/MoS₂/CoPi) is similar to that of CdS/MoS₂/CoPi except that CdS was washed.

Synthesis of CdS/CoPi. 50 mg CdS was dispersed in a 30 mL neutral buffer aqueous solution containing 0.1 M sodium phosphate and a certain amount of 0.02 M cobalt nitrate hexahydrate ($\text{Co}(\text{NO}_3)_2 \cdot 6\text{H}_2\text{O}$). After nitrogen degassing for 30 min, the suspension was illuminated with visible light for 3 h in nitrogen atmosphere. After that, the sample was collected by centrifugation, washed with water and ethanol three times, respectively, and dried at 80 °C in air.

n ACKNOWLEDGMENTS

This work was financially supported by National Natural Science Foundation of China (22102002, 52072001, 51872003) and Natural Science Foundation of Anhui Province (2108085QE192).

n AUTHOR CONTRIBUTION

X. Zhang and G. Zhao contributed equally to this work.

n AUTHOR INFORMATION

Corresponding authors. Emails: jdczlx@ahu.edu.cn and yupengyuan@ahu.edu.cn

n COMPETING INTERESTS

The authors declare no competing interests.

n ADDITIONAL INFORMATION

Supplementary information is available for this paper at <http://manu30.magtech.com.cn/jghx/EN/10.14102/j.cnki.0254-5861.2022-0168>.

For submission: <https://www.editorialmanager.com/cjschem>

n REFERENCES

- (1) Zhang, M.; Nie, S.; Cheng, T.; Feng, Y.; Zhang, C.; Zheng, L.; Wu, L.; Hao, W.; Ding, Y. Enhancing the macroscopic polarization of CdS for piezo-photocatalytic water splitting. *Nano Energy* **2021**, 90, 106635.
- (2) Bai, Y.; Hippalgaonkar, K.; Sprick, R. S. Organic materials as photocatalysts for water splitting. *J. Mater. Chem. A* **2021**, 9, 16222-16232.
- (3) Dai, C.; Pan, Y.; Liu, B. Conjugated polymer nanomaterials for solar water splitting. *Adv. Energy Mater.* **2020**, 10, 2002474.
- (4) Chen, S.; Takata, T.; Domen, K. Particulate photocatalysts for overall water splitting. *Nat. Rev. Mater.* **2017**, 2, 17050.
- (5) Xu, J.; Zhong, W.; Gao, D.; Wang, X.; Wang, P.; Yu, H. Phosphorus-enriched platinum diphosphide nanodots as a highly efficient cocatalyst for photocatalytic H₂ evolution of CdS. *Chem. Eng. J.* **2022**, 439, 135758.

- (6) He, J.; Hu, L.; Shao, C.; Jiang, S.; Sun, C.; Song, S. Photocatalytic H₂O overall splitting into H₂ bubbles by single atomic sulfur vacancy CdS with spin polarization electric field. *ACS Nano* **2021**, 15, 18006-18013.
- (7) Tian, L.; Min, S.; Wang, F. Integrating noble-metal-free metallic vanadium carbide cocatalyst with CdS for efficient visible-light-driven photocatalytic H₂ evolution. *Appl. Catal. B* **2019**, 259, 118029.
- (8) Han, G.; Jin, Y.-H.; Burgess, R. A.; Dickenson, N. E.; Cao, X.-M.; Sun, Y. Visible-light-driven valorization of biomass intermediates integrated with H₂ production catalyzed by ultrathin Ni/CdS nanosheets. *J. Am. Chem. Soc.* **2017**, 139, 15584-15587.
- (9) Li, K.; Han, M.; Chen, R.; Li, S.-L.; Xie, S.-L.; Mao, C.; Bu, X.; Cao, X.-L.; Dong, L.-Z.; Feng, P.; Lan, Y.-Q. Hexagonal@cubic CdS core@shell nanorod photocatalyst for highly active production of H₂ with unprecedented stability. *Adv. Mater.* **2016**, 28, 8906-8911.
- (10) Li, C.-Q.; Du, X.; Jiang, S.; Liu, Y.; Niu, Z.-L.; Liu, Z.-Y.; Yi, S.-S.; Yue, X.-Z. Constructing direct Z-Scheme heterostructure by enwrapping ZnIn₂S₄ on CdS hollow cube for efficient photocatalytic H₂ generation. *Adv. Sci.* **2022**, n/a, 2201773.
- (11) Xiang, X.; Zhu, B.; Cheng, B.; Yu, J.; Lv, H. Enhanced photocatalytic H₂-production activity of CdS quantum dots using Sn²⁺ as cocatalyst under visible light irradiation. *Small* **2020**, 16, 2001024.
- (12) Feng, R.; Wan, K.; Sui, X.; Zhao, N.; Li, H.; Lei, W.; Yu, J.; Liu, X.; Shi, X.; Zhai, M.; Liu, G.; Wang, H.; Zheng, L.; Liu, M. Anchoring single Pt atoms and black phosphorene dual co-catalysts on CdS nanospheres to boost visible-light photocatalytic H₂ evolution. *Nano Today* **2021**, 37, 101080.
- (13) Shao, M.; Shao, Y.; Ding, S.; Tong, R.; Zhong, X.; Yao, L.; Ip, W. F.; Xu, B.; Shi, X.-Q.; Sun, Y.-Y.; Wang, X.; Pan, H. Carbonized MoS₂: superactive co-catalyst for highly efficient water splitting on CdS. *ACS Sustain. Chem. Eng.* **2019**, 7, 4220-4229.
- (14) Sun, Q.; Wang, N.; Yu, J.; Yu, J. C. A hollow porous CdS photocatalyst. *Adv. Mater.* **2018**, 30, 1804368.
- (15) Yin, M.; Zhang, W.; Qiao, F.; Sun, J.; Fan, Y.; Li, Z. Hydrothermal synthesis of MoS₂-NiS/CdS with enhanced photocatalytic hydrogen production activity and stability. *J. Solid State Chem.* **2019**, 270, 531-538.
- (16) He, B.; Bie, C.; Fei, X.; Cheng, B.; Yu, J.; Ho, W.; Al-Ghamdi, A. A.; Wageh, S. Enhancement in the photocatalytic H₂ production activity of CdS NRs by Ag₂S and NiS dual cocatalysts. *Appl. Catal. B* **2021**, 288, 119994.
- (17) Di, T.; Deng, Q.; Wang, G.; Wang, S.; Wang, L.; Ma, Y. Photodeposition of CoO_x and MoS₂ on CdS as dual cocatalysts for photocatalytic H₂ production. *J. Mater. Sci. Technol.* **2022**, 124, 209-216.
- (18) Yang, H.; Jin, Z.; Wang, G.; Liu, D.; Fan, K. Light-assisted synthesis MoS_x as a noble metal free cocatalyst formed heterojunction CdS/Co₃O₄ photocatalyst for visible light harvesting and spatial charge separation. *Dalton Trans.* **2018**, 47, 6973-6985.
- (19) Hu, X.; Jin, J.; Wang, Y.; Lin, C.; Wan, S.; Zhang, K.; Wang, L.; Park, J. H. Au/MoS₂ tips as auxiliary rate aligners for the photocatalytic generation of syngas with a tunable composition. *Appl. Catal. B* **2022**, 308, 121219.
- (20) Lin, K.; Feng, L.; Li, D.; Zhang, J.; Wang, W.; Ma, B. Improved photocatalytic hydrogen evolution on (Ru/WC)/CdS via modulating the transferring paths of photo-excited electrons. *Appl. Catal. B* **2021**, 286, 119880.
- (21) Lu, K.-Q.; Qi, M.-Y.; Tang, Z.-R.; Xu, Y.-J. Earth-abundant MoS₂ and cobalt phosphate dual cocatalysts on 1D CdS nanowires for boosting photocatalytic hydrogen production. *Langmuir* **2019**, 35, 11056-11065.
- (22) Qiu, B.; Cai, L.; Zhang, N.; Tao, X.; Chai, Y. A ternary dumbbell

structure with spatially separated catalytic sites for photocatalytic overall water splitting. *Adv. Sci.* **2020**, 7, 1903568.

(23) Zhang, K.; Qian, S.; Kim, W.; Kim, J. K.; Sheng, X.; Lee, J. Y.; Park, J. H. Double 2-dimensional H₂-evolving catalyst tipped photocatalyst nano-wires: a new avenue for high-efficiency solar to H₂ generation. *Nano Energy* **2017**, 34, 481-490.

(24) Khan, K.; Tao, X.; Zhao, Y.; Zeng, B.; Shi, M.; Ta, N.; Li, J.; Jin, X.; Li, R.; Li, C. Spatial separation of dual-cocatalysts on one-dimensional semiconductors for photocatalytic hydrogen production. *J. Mater. Chem. A* **2019**, 7, 15607-15614.

(25) Kwon, G.; Jang, H.; Lee, J.-S.; Mane, A.; Mandia, D. J.; Soltan, S. R.; Utschig, L. M.; Martinson, A. B. F.; Tiede, D. M.; Kim, H.; Kim, J. Resolution of electronic and structural factors underlying oxygen-evolving performance in amorphous cobalt oxide catalysts. *J. Am. Chem. Soc.* **2018**, 140, 10710-10720.

(26) Yue, Q.; Wan, Y.; Sun, Z.; Wu, X.; Yuan, Y.; Du, P. MoP is a novel, noble-metal-free cocatalyst for enhanced photocatalytic hydrogen production from water under visible light. *J. Mater. Chem. A* **2015**, 3, 16941-

16947.

(27) Jiang, D.; Sun, Z.; Jia, H.; Lu, D.; Du, P. A cocatalyst-free CdS nanorod/ZnS nanoparticle composite for high-performance visible-light-driven hydrogen production from water. *J. Mater. Chem. A* **2016**, 4, 675-683.

(28) Cao, H.; Wang, T.; Li, J.; Wu, J.; Du, P. A molecular cobaloxime cocatalyst and ultrathin FeOOH nanolayers co-modified BiVO₄ photoanode for efficient photoelectrochemical water oxidation. *J. Energy Chem.* **2022**, 69, 497-505.

(29) Zhu, M.; Zhai, C.; Kim, S.; Fujitsuka, M.; Majima, T. Monitoring transport behavior of charge carriers in a single CdS@CuS nanowire via in situ single-particle photoluminescence spectroscopy. *J. Phys. Chem. Lett.* **2019**, 10, 4017-4024.

Received: July 10, 2022

Accepted: August 16, 2022

Published online: August 18, 2022

Published: September 22, 2022